

Gas-particle Partitioning and Hydrolysis of Organic Nitrates Formed from the Oxidation of α -Pinene in Environmental Chamber Experiments

J. K. Bean and L. Hildebrandt Ruiz

McKetta Department of Chemical Engineering, The University of Texas at Austin, Austin, Texas

Correspondence to L. Hildebrandt Ruiz (lhr@che.utexas.edu)

Abstract

Gas-particle partitioning and hydrolysis of organic nitrates (ON) influences their role as sinks and sources of NO_x and their effects on the formation of tropospheric ozone and organic aerosol (OA). In this work organic nitrates were formed from the photo-oxidation of α -pinene in environmental chamber experiments under different conditions. Particle-phase ON hydrolysis rates consistent with observed ON decay exhibited a nonlinear dependence on relative humidity (RH): an ON decay rate of 2 day^{-1} was observed when the RH ranged between 20 and 60%, and no significant ON decay was observed at RH lower than 20%. In experiments when the highest observed RH exceeded the deliquescence RH of the ammonium sulfate seed aerosol, the particle-phase ON decay rate was as high as 7 day^{-1} and more variable. The ON gas-particle partitioning was dependent on total OA concentration and temperature, consistent with absorptive partitioning theory. In a volatility basis set the ON partitioning was consistent with mass fractions of [0 0.11 0.03 0.86] at saturation mass concentrations (C^*) of [1 10 100 1000] $\mu\text{g m}^{-3}$.

1 Introduction

Organic nitrates (ON) play an important role in atmospheric chemistry as they can act as sinks and sources of NO_x ($\text{NO} + \text{NO}_2$) and thereby affect the formation of tropospheric ozone and organic aerosol. The sink reaction – addition of NO to a peroxy radical ($\text{R-O-O}\cdot$) to form an organic nitrate (R-O-NO_2) – breaks the $\cdot\text{OH}$ initiated oxidation cycle and reduces the formation of ozone (Seinfeld and Pandis, 2006). Most R-O-NO_2 molecules are semi-volatile and are therefore expected to partition between the gas and particle phases. They can be transported in either phase and can become a source of NO_x when they are photolyzed or oxidized, contributing to the regional nature of NO_x pollution. Attempts to implement organic nitrate decomposition reactions in a chemical transport model which did not account for gas-particle partitioning of organic nitrates resulted in over-prediction of NO_x and ozone concentrations (Yarwood et al., 2012), consistent with an over-estimate of the strength of organic nitrates as NO_x sources.

Recent studies have suggested that organic nitrates in the condensed phase may undergo hydrolysis, leading to the formation of HNO_3 (Day et al., 2010; Darer et al., 2011; Hu et al., 2011; Liu et al., 2012; Browne et al., 2013; Jacobs et al., 2014; Rindelaub et al., 2015). This is a more permanent sink for NO_x and would decrease the regeneration of NO_x from organic nitrates. While these studies have found

35 evidence for hydrolysis of aerosol-phase organic nitrates (ON^{aer}), it is not clear at which rate ON
36 hydrolysis occurs. Correctly modeling organic nitrates and ozone formation depends on knowledge of
37 the ON partitioning and hydrolysis rate.

38 While ON hydrolysis in the bulk phase has been studied for decades (Baker and Easty, 1950; Baker and
39 Easty, 1952; Boschan et al., 1955), organic nitrate hydrolysis in atmospheric particles has only recently
40 started to receive attention. Day et al. (2010) observed a decrease in particulate organic nitrates
41 measured in coastal southern California under acidic conditions at high relative humidity and
42 hypothesized hydrolysis as the cause. Browne et al. (2013) used ON hydrolysis to justify observations
43 over the Boreal Forest of higher levels of HNO_3 despite higher production rates of organic nitrates. The
44 chamber experiments (0 to >80% RH) performed by Liu et al. (2012) using trimethylbenzene (an
45 anthropogenic volatile organic compound) and HONO as oxidant were the first to measure the
46 hydrolysis of condensed organic nitrates. Rindelaub et al. (2015) observed ON hydrolysis while
47 measuring partitioning of α -pinene SOA but did not directly quantify it. Boyd et al. (2015) measured
48 hydrolysis of ON formed from nitrate radical oxidation of β -pinene.

49 The partitioning of organic nitrates to the particle phase is important to determine their fate as only
50 condensed organic nitrates are expected to hydrolyze appreciably to HNO_3 . Absorptive partitioning
51 theory (Pankow, 1994; Donahue et al., 2006, Rollins et al., 2013; Rindelaub et al., 2015) has been used
52 to describe the gas-particle partitioning of organic nitrates. Rollins et al. (2013) used partitioning data
53 from the 2010 CalNex campaign to find a volatility basis set distribution for ON observed at ambient
54 aerosol concentrations. Rindelaub et al. (2015) observed the partitioning of organic nitrates formed
55 from the $\cdot\text{OH}$ initiated oxidation of α -pinene at various levels of relative humidity. However, other work
56 has suggested that the partitioning of organic nitrates to the particle phase is irreversible (Perraud et al.,
57 2012). The goals of this work were to form organic nitrates in controlled environmental chamber
58 experiments from the $\cdot\text{OH}$ -dominated oxidation of α -pinene under high NO_x conditions and various
59 relative humidity levels and:

- 60 1. Quantify the hydrolysis rate of organic nitrates.
- 61 2. Verify whether the gas-particle partitioning of organic nitrates is reversible and can therefore be
62 modeled by absorptive partitioning theory
- 63 3. Parameterize the gas-particle partitioning of organic nitrates

64 **2 Methods**

65 **2.1 Environmental Chamber Experiments**

66 All experiments were performed in the Atmospheric Physicochemical Processes Laboratory Experiments
67 (APPLE) chamber located at the University of Texas at Austin (UT-Austin). The APPLE chamber is a ~ 12
68 m^3 Teflon[®] bag suspended inside of a temperature-controlled room. The walls of the room are lined
69 with UV lights which can be used to induce photolysis reactions. The intensity of the UV lights has been
70 characterized by the photolysis rate of NO_2 , which was measured to be 0.4 min^{-1} , similar to ambient NO_2

71 photolysis rates (e.g., 0.46 min^{-1} at a zenith angle of 40° , Carter et al., 2005). Before each experiment the
72 bag was flushed for at least 12 hours with clean air from an Aadco clean air generator (Model 737-14A)
73 at a flow rate exceeding 100 liters per minute (LPM). Ammonium sulfate ($(\text{NH}_4)_2\text{SO}_4$) particles (Fisher
74 Scientific, 99.5%) were injected both to monitor wall loss rates (Hildebrandt et al., 2009) as well as to act
75 as seed particles onto which organic vapors can condense. Gas phase NO was injected directly into the
76 chamber from a cylinder (Airgas, 9.94 PPM $\pm 2\%$) and liquid-phase α -pinene (Sigma Aldrich, 98%) was
77 injected to a glass bulb and subsequently evaporated into the chamber with a steady stream of mildly
78 heated air. H_2O_2 , which photolyzes to $2 \cdot\text{OH}$, was used as $\cdot\text{OH}$ radical source and was either injected by
79 bubbling air through an aqueous H_2O_2 solution (Fisher Scientific, 30% weight) or by injecting H_2O_2
80 solution into a glass bulb and subsequently evaporating it into the chamber with a steady stream of
81 mildly heated air. Some experiments were performed under dry conditions ($<5\%$ relative humidity); in
82 other experiments humidity was increased by passing air through clean water and then into the
83 chamber. Experimental conditions and results are summarized in Table 1. Results are discussed in Sect.
84 3.

85 Reactions were allowed to proceed for at least 4 hours with continuous UV light. Experiments were run
86 in a batch mode with no injections or dilution after the experiment was started; the bag volume of 12
87 m^3 allowed ample time for sampling. In some cases the temperature effects on gas-particle partitioning
88 were observed by increasing temperature to 40°C in the chamber after the UV lights had been turned
89 off (see Sect. 3.2).

90

91 **2.1.1 Instrumentation**

92 The composition of PM_{10} (particulate matter smaller than 1 micrometer in diameter) was measured using
93 an Aerosol Chemical Speciation Monitor (ACSM) from Aerodyne Research Inc. (Ng et al., 2011). In the
94 ACSM, particles are flash-vaporized on a heater at 600°C , and the resulting gas molecules are ionized
95 using electron-impact ionization. This harsh ionization method results in fragmentation of most
96 molecules. The molecular fragments, which are measured by a quadrupole mass spectrometer, are
97 attributed to four categories—organics, nitrate, sulfate, and ammonium - using a fragmentation table
98 (Allan et al., 2004). The instrument alternates between normal sampling and sampling through a particle
99 filter, enabling subtraction of a gas-phase background. During this study the ACSM was operated at a
100 time resolution (filter/sample cycle length) of approximately 90 seconds. The size distribution of
101 particles was measured using a Scanning Electrical Mobility System (SEMS) from Brechtel
102 Manufacturing, Inc. The SEMS uses a Differential Mobility Analyzer (DMA) to size-select particles based
103 on their electric mobility, which are then counted by a Condensation Particle Counter (CPC). The DMA
104 continuously cycled between the voltages which select particles ranging from 5 to 1000 nm in diameter,
105 resulting in a time resolution of the particle size distribution of approximately 60 seconds.

106 Gas phase reaction products were monitored using a High-Resolution Time-of-Flight Chemical Ionization
107 Mass Spectrometer (HR-ToF-CIMS) from Aerodyne Research, Inc.. The HR-ToF-CIMS uses softer chemical
108 ionization which results in minimal fragmentation of parent molecules. Mass spectra are derived from
109 measurements of the ions' time-of-flight as they are pulsed through a low pressure chamber in a "V"

110 shape. Two chemical reagent ions were used—water clusters ($\text{H}_3\text{O}^+\cdot(\text{H}_2\text{O})_n$) and iodide-water clusters (I^-
111 $\cdot(\text{H}_2\text{O})_n$). Water cluster ionization is most sensitive towards detection of moderately oxidized
112 hydrocarbons; the ability to ionize and thus sensitivity is based on the relative proton affinity between
113 the water cluster and the parent molecule (Lindinger et al., 1998). This method was used to monitor α -
114 pinene as well as early-generation oxidation products. Iodide-water cluster ionization is most sensitive
115 towards detection of more highly oxidized hydrocarbons; this method was used to observe later-
116 generation oxidation products as well as HNO_3 and H_2O_2 . In the work presented here data from the HR-
117 ToF-CIMS are only used qualitatively since, as it was later discovered, a partially clogged inlet may have
118 interfered with instrument calibration and quantitative measurements.

119 Concentrations of NO and O_3 were measured using Teledyne chemiluminescence NO_x and absorption O_3
120 monitors (200E and 400E, respectively); concentrations of NO_2 were measured via an NO_2 monitor from
121 Environnement (Model AS32M), which uses a Cavity Attenuated Phase Shift (CAPS) method to directly
122 measure NO_2 (Kebabian et al., 2008). The advantage of this direct NO_2 measurement is that it does not
123 rely on NO_2 conversion to NO and therefore does not suffer from interference by other oxidized
124 nitrogen compounds such as HONO and organic nitrates (Winer et al., 1974).

125 2.1.2 Data Analysis

126 Data from the ACSM were analyzed in Igor Pro using the software package “ACSM Local,” which includes
127 a correction for relative ion transmission efficiency as well as changes in the flow rate throughout the
128 experiment. The SEMS volume concentration was converted to mass using the densities 1.77 g/cm^3 for
129 ammonium sulfate and 1.4 g/cm^3 for organics and organic nitrates (Ng et al., 2007). The time series of
130 particle mass concentration (not corrected for wall losses) during Expt. 7 is shown in Fig. S1; other
131 experiments exhibited similar time series.

132 All PM nitrate was assumed to be organic because no inorganic nitrate was introduced in these
133 controlled experiments. PM nitrate is measured by the ACSM as NO^+ and NO_2^+ fragments, and the
134 standard fragmentation table is used to estimate the portion of the m/z 30 that is due to NO^+ (as
135 opposed to $(^{15}\text{N})_2^+$ or Organics). Nitric acid is formed in the gas phase as well as in the particle phase
136 through hydrolysis, but it is assumed that nitric acid concentrations are negligible in the particle phase
137 due to its high vapor pressure (Fry et al., 2009). A Henry’s Law calculation suggests that the total amount
138 of aqueous HNO_3 in particles is 3 orders of magnitude lower than that in the gas phase.

139 The ACSM does not detect all sampled particles, primarily due to particle bounce at the vaporizer,
140 resulting in a collection efficiency (CE) smaller than 1. Collection efficiency and wall losses were
141 accounted for simultaneously by multiplying the ACSM concentrations of organics and organic nitrates
142 by the mass concentration ratio $C_{SEMS}^{t=0}/C_{ACSM}^{seed}(t)$ as has been done in previous work (Hildebrandt et al.,
143 2009). Here, $C_{SEMS}^{t=0}$ is the mass concentration of ammonium sulfate seed just before the UV lights are
144 turned on and organic aerosol formation commences and $C_{ACSM}^{seed}(t)$ is the time dependent mass
145 concentration of $(\text{NH}_4)_2\text{SO}_4$ measured by the ACSM throughout the experiment. This correction assumes
146 that particles on the chamber walls participate in gas-particle partitioning as though they are still in
147 suspension and that the suspended ammonium sulfate concentration changes only due to wall losses. It

148 accounts for partitioning of organic vapors into wall-deposited particles (Hildebrandt et al., 2009) but
149 does not account for losses of organic vapors onto the clean Teflon® walls (e.g. Matsunaga and Ziemann,
150 2010).

151 The ACSM standard fragmentation table was adjusted based on filter measurements taken in each
152 experiment as described in the supplementary information. Data from the HR-ToF-CIMS were analyzed
153 in Igor Pro (Wavemetrics) using Tofware, the software provided with the instrument. The data were first
154 mass calibrated based on HR-ToF-CIMS reagent ions and other known ions. The baseline was subtracted
155 and the average peak shape was found so it could be used for high resolution analysis, through which
156 multiple ions can be identified at any given integer m/z . Ions up to m/z 300 were analyzed in high
157 resolution mode. Only prominent ions were fit above m/z 200 because of the high number of possible
158 ions at this high m/z . After ions were identified in the high resolution spectrum, the peaks were
159 integrated to yield a time series of ions. Analyte ion concentrations were then normalized by the
160 reagent ion concentrations – the sum of H_3O^+ , $\text{H}_3\text{O}^+ \cdot (\text{H}_2\text{O})$ and $\text{H}_3\text{O}^+ \cdot (\text{H}_2\text{O})_2$ for water cluster ionization
161 and the sum of I^- and $\text{I}^- \cdot (\text{H}_2\text{O})$ for iodide-cluster ionization. This correction accounts for changes in
162 reagent ion concentrations and instrument sensitivity during and between experiments. Relative
163 humidity can affect instrument sensitivity but this varied by less than 5% during each experiment.

164 The partitioning coefficient of a species is defined as the ratio of the species concentration in the
165 particle phase to the total species concentration (gas and particle phase). For a single compound the
166 partitioning coefficient is the same whether it is on a mass or mole basis. However, for a mix of
167 compounds, such as those formed in -OH-initiated oxidation, the mass and mole-basis partitioning
168 coefficients will be different, with the coefficient expected higher on a mass basis since higher molecular
169 weight compounds typically have lower vapor pressure. The partitioning coefficient in this work was
170 calculated on a mole basis, in part because fragmentation in the ACSM makes it impossible to tell the
171 original size and identity of ON molecules. This mole-basis partitioning coefficient is also more useful for
172 most modeling efforts which group chemical species without knowledge of their exact molecular
173 identity. The particle-phase ON concentration was quantified using data from the ACSM: the mass
174 concentration of nitrate measured by the ACSM was converted to mixing ratio (ppb) using the molecular
175 weight of the nitrate functional group (62 g/mol). This assumes that the ON have only one nitrate
176 functional group. Conversion of the nitrate mass concentration to mixing ratio avoids the need to
177 assume an ON molecular weight (needed to estimate ON mass concentrations from ACSM) and is
178 therefore deemed to be a more accurate measure of ON from the ACSM. Quantification of all gas phase
179 ON species would necessitate calibration and identification of all ON species which is not feasible.
180 Instead, a chamber box model and nitrogen balance was employed to estimate total gas-phase ON as
181 described below.

182 **2.2 Chamber Modeling and Partitioning Coefficient**

183 In these experiments only five major forms of oxidized nitrogen are present in significant
184 concentrations—NO, NO₂, HNO₃, ON^{gas} and ON^{aer} (gas and aerosol-phase organic nitrates, respectively).
185 Figure S2 shows that, based on the Statewide Air Pollution Research Center (SAPRC) model
186 (<http://www.engr.ucr.edu/~carter/SAPRC/>), the concentrations of other forms of reactive nitrogen are
187 orders of magnitude lower than the concentrations of these five forms. Concentrations of NO and NO₂

188 were measured using gas-phase monitors, ON^{aer} was measured using the ACSM, and concentrations of
 189 HNO_3 were approximated using the SAPRC box model. The concentration of ON^{gas} was then calculated
 190 based on a nitrogen mass balance ($\text{ON}^{\text{gas}} = \text{NOx}^{\text{initial}} - \text{NO}_2 - \text{NO} - \text{ON}^{\text{aer}} - \text{HNO}_3^{\text{model}}$), and the partitioning
 191 coefficient was calculated as a time series for each experiment.”

192 The concentration of H_2O_2 used in the model was adjusted until the modeled NO , NO_2 , and O_3
 193 concentrations closely matched those measured throughout each experiment as shown in Fig. S3 for
 194 Expt. 7. In Expts. 1, 2, and 3 (which were used to calculate the volatility basis set parameters) H_2O_2 was
 195 injected by passing air through a solution of H_2O_2 and into the chamber, and the amount of H_2O_2
 196 injected could not be estimated. In later experiments H_2O_2 was directly injected into the chamber
 197 through evaporation of a known liquid volume of solution, and the estimated amount of H_2O_2 injected
 198 was about half of the H_2O_2 concentrations consistent with observed NO , NO_2 and O_3 based on the
 199 model. This difference may be due to inefficient injection or uncertainties in the UV spectrum. The
 200 absorption cross section of H_2O_2 only minimally intersects with the emission spectrum of the UV lights
 201 used in this chamber. Thus, small changes in the UV spectrum (or errors in measurements of the
 202 spectrum) could cause significant errors in estimated concentrations of $[\text{OH}]$, which drive the observed
 203 concentrations of NO , NO_2 and O_3 .

204 SAPRC simulations were conducted with the reaction mechanism Carbon Bond 6 revision 2 (CB6r2),
 205 which includes organic nitrate hydrolysis through a rate estimated from a combination of the work of Liu
 206 et al. (2012) and Rollins et al. (2013); updates to CB6r2 were described by Hildebrandt Ruiz and Yarwood
 207 (2013). Experiments were modeled with and without organic nitrate hydrolysis to see the effect this has
 208 on the predicted ON partitioning coefficient. The overall effect of this process was small, with a
 209 maximum effect being a 5% decrease to the partitioning coefficient by removing the hydrolysis
 210 mechanism from the model. This corresponded to a 17% decrease in HNO_3 , which suggests that the
 211 partitioning coefficient estimated in this work is not very sensitive to changes in the modeled HNO_3
 212 concentrations. For the results and analysis presented here the HNO_3 concentrations were taken from
 213 CB6r2 with the inclusion of the ON hydrolysis process for experiments above 20% RH and without the
 214 hydrolysis process for experiments below 20% RH.

215 According to absorptive partitioning theory (Pankow, 1994; Donahue et al., 2006), the gas-particle
 216 partitioning of an organic species depends on its vapor pressure and the concentration of organic
 217 material in the particle phase. The fraction of a compound i in the particle phase (Y_i) is given by
 218 (Donahue et al., 2006):

$$219 \quad Y_i = \left(1 + \frac{C_i^*}{C_{OA}}\right)^{-1} \quad (1)$$

220 where C_{OA} is the organic aerosol concentration and C_i^* is the saturation mass concentration of species i
 221 (the saturation vapor pressure converted to concentration units). In the volatility basis set (VBS,
 222 Donahue et al., 2006), organic species are lumped by C_i^* spaced logarithmically. This leads to an overall
 223 partitioning coefficient

$$224 \quad Y_{tot} = \sum_{i=1}^n F_i \left(1 + \frac{C_i^*}{C_{OA}}\right)^{-1} \quad (2)$$

225 (Rollins et al., 2013), where F_i is the fraction of organic species in the volatility bin described by C_i^* . In
226 this work we used measurements of C_{OA} and Y_{tot} to fit the F_i using a Matlab optimization routine. These
227 VBS parameters can be used in models to represent the gas-particle partitioning of organic nitrates and
228 account for changes in partitioning with temperature and C_{OA} .

229 **3 Results and Discussion**

230 A typical time series of compounds containing oxidized nitrogen is shown in Fig. 1 (Expt. 7). Initially the
231 chamber contains only NO and a small amount of NO₂, in addition to α -pinene and inorganic seed
232 aerosol. When the UV lights are activated at time = 0 the NO immediately begins to react with \cdot OH and
233 other radicals to form NO₂ and additional NO_y compounds such as organic nitrates. Ozone formation
234 also starts and thus in these experiments ozone also plays a role in the oxidation of α -pinene. Based on
235 the SAPRC model 15% of the total α -pinene reacts with ozone while the rest reacts with \cdot OH. Table 1
236 summarizes results from all experiments. Concentrations of O₃, ON^{aer}, PM organics, and ON^{gas} are
237 averaged over approximately 20 minutes of the time when PM organics and nitrates peak in
238 concentration. This averaging period was chosen so that experiments with different H₂O₂ concentrations
239 could be compared even though they reach their maximum concentrations at different rates. Higher
240 initial loading of NO_x, α -pinene, and H₂O₂ resulted in higher concentrations of ozone and PM.

241 Figure 2 shows time series of molecular ions identified using the HR-ToF-CIMS using water cluster
242 (“positive mode”) and iodide-water cluster (“negative mode”) ionization. Many compounds are
243 identified with the CIMS and a select few of the most prominent compounds were chosen for Fig. 2. In
244 short time periods after switching reagent ions the sensitivity of the HR-ToF-CIMS slowly adjusts to a
245 steady state value. Minor changes during these short time periods should be taken with caution but the
246 overall trends over the 4.5 hour experiment are useful in viewing oxidation trends. The initial data
247 collected in negative mode show that formation of organic nitrates begins immediately after oxidation
248 has started. Later in the experiment the less-oxygenated compounds observed in positive mode begin to
249 decrease while the more highly oxygenated compounds observed in negative mode continue to
250 increase, consistent with oxidation and conversion of less oxidized compounds to more highly oxidized
251 compounds continuing throughout the experiment. Highly oxidized compounds which still contain ten
252 carbon atoms (as the precursor α -pinene) begin to decrease towards the end of the experiment while
253 fragmented compounds (containing less than ten carbon atoms) continue to increase, consistent with
254 fragmentation of the carbon backbone during oxidation. Molecular weights of the gas-phase compounds
255 identified here range from 221 to 279 g mol⁻¹ and align well with the range of molecular weights
256 estimated by Fry et al. (2009) for particle-phase organic nitrates formed from NO₃ oxidation of β -pinene
257 (229±12 to 434±25 g mol⁻¹). Gas-phase organic nitrates identified here are therefore expected to be
258 semi-volatile and to partition significantly to the particle phase.

259 **3.1 Hydrolysis of Organic Nitrates**

260 Concentrations of wall-loss corrected (normalized to sulfate) PM nitrate were observed to decrease at
261 the end of most experiments. These decreases of PM nitrate are attributed to physical or chemical
262 processes in the gas and aerosol phases, and an exponential decay was fit to the data to quantify the

263 decay. The exception was experiments 1 and 3 during which production of SOA was slow (primarily due
264 to lower initial H₂O₂ and α -pinene) and continued throughout the experiment, so a decay could not be
265 observed. Examples of the decay for a humid and dry experiment are shown in Fig. S4. The decay rates
266 for each experiment are reported in Table 1 and appear to depend on relative humidity as shown in Fig.
267 3. When the RH ranged between 20 and 60%, an ON decay rate of 2 day⁻¹ was observed; no significant
268 ON decay was observed at RH lower than 20%. Experiments conducted at an average RH of 67% or
269 higher can exhibit a significantly higher decay rate, probably due to effects of being near the
270 deliquescence relative humidity of the ammonium sulfate seed aerosol. In experiments 10 and 12, which
271 have decay rates well above 2 day⁻¹, the chamber was initially cooled to 20 °C before the UV lights were
272 turned on. Once the UV lights were activated the temperature then increased to 25 °C and the RH
273 settled at the values indicated in Table 1. For these experiments the RH was above 80% (the
274 deliquescence RH, DRH, of (NH₄)₂SO₄ for several minutes, potentially resulting in aqueous aerosol.
275 Experiment 11 also reached a relative humidity above deliquescence, yet it shows a lower nitrate loss
276 rate than Expts. 10 and 12. The ratio of organics and nitrates to sulfate (seed) particles was much lower
277 in Expt. 11 compared to Expts. 10 and 12, but whether and why this would result in a different nitrate
278 loss rate is currently unclear. The relative humidity in Expt. 4 did not reach the DRH of (NH₄)₂SO₄. Future
279 work should focus on the fate of ON at higher (> 60%) relative humidity. The generally higher nitrate loss
280 rate at higher RH makes hydrolysis of particulate nitrate functional groups the most plausible
281 explanation for the observed decay.

282 PM organics also decreased in some experiments, but their loss rate was lower and more variable than
283 that of nitrate. Based on the work by Chuang et al. (2015) the addition of a nitrate functional group
284 decreases volatility of a compound by 2.5 orders of magnitude – slightly more than the substituted
285 alcohol group from hydrolysis. Thus, the organic compound resulting from ON is more volatile than the
286 original organic nitrate, and as a result could partition to the gas phase, resulting in a decrease in PM
287 organics.

288 No direct observation of hydrolysis (conversion of the -ONO₂ group to an -OH group) has been made in
289 this or previous work. The estimated hydrolysis lifetime of 12 hours (loss rate of 2 day⁻¹) for particulate
290 organic nitrates is similar to hydrolysis rates suggested by other studies under humid conditions. Liu et
291 al. (2012) observed a trend similar to that shown in Fig. 3 in chamber experiments in which ON were
292 formed from the oxidation of tri-methyl benzene using HONO as the ·OH and NO_x source. In those
293 experiments, PM nitrate was found to have negligible loss rate below 20% RH but a lifetime of 6 hours at
294 40% RH and higher. Perring et al. (2009) estimated the lifetime of isoprene nitrates to be between 95
295 minutes and 16 hours depending on their branching ratio in isoprene ·OH oxidation. Boyd et al. (2015)
296 measured a lifetime of 3-4.5 hours for 10% of ON formed from NO₃ oxidation of β -pinene, with a much
297 longer lifetime for the remaining 90%. This suggests that 10% of the ON functional groups were tertiary
298 with the rest being primary or secondary as those have been shown to hydrolyze much slower in the
299 bulk phase (Darer et al., 2011; Hu et al., 2011). More tertiary ON groups are expected from α -pinene
300 than β -pinene, based on the location of the double bond.

301 Similar VOC precursors such as α -pinene and β -pinene can form different fractions of primary/secondary
302 and tertiary ON. When NO₃ reacts and bonds with the terminal double bond of β -pinene, an alkyl radical

303 is formed in either a primary or tertiary position (opposite of the carbon-nitrate bond). The tertiary alkyl
304 radical is more stable, so primary organic nitrates are expected to be more abundant. The double bond
305 in α -pinene is not terminal, so the NO_3 reaction produces either a secondary or tertiary ON and alkyl
306 radical. NO_3 typically bonds with the less substituted carbon of a double bond so that a more highly
307 substituted alkyl radical is formed. The reverse is true for $\text{OH}+\text{NO}$ chemistry. In this case NO reacts with
308 the peroxy-radical to form the nitrate group. The peroxy-radical, a product of O_2 and an alkyl radical, is
309 likely to be on a more substituted carbon as this would have been the more stable alkyl radical. Thus,
310 more highly substituted ON are expected from $\text{OH} + \text{NO}_x$ than from NO_3 chemistry. This has important
311 implications for attempts to model ON and the resulting NO_x recycling.

312 As Table 1 shows experiments were conducted at varying NO_x and α -pinene concentrations, relative
313 humidity, and hydrogen peroxide ($\cdot\text{OH}$ radical source) levels, which resulted in different final
314 concentrations of PM nitrate and total OA. Liu et al. (2012) suggested that a lower PM nitrate / OA ratio
315 at higher RH could be due to ON hydrolysis. In these experiments, the correlation between the ratio of
316 PM nitrate/total OA (measured when total OA was highest) and RH was very low ($R^2 = 0.02$). Thus, based
317 on these experiments, differences in the observed final PM nitrate / OA are due to experimental
318 conditions other than relative humidity.

319 **3.2 Gas-particle Partitioning of Organic Nitrates**

320 In order to test the reversibility of ON partitioning the temperature of the chamber was increased after
321 OA had formed (and when the UV lights were off) in some experiments. Figure 4 shows gas and particle-
322 phase measurements taken from a representative experiment (Expt. 2). After the UV lights are turned
323 off there is a 60 minute period in which the temperature stabilizes around 15 °C. This is followed by ~90
324 minutes of heating to a final temperature of 45 °C. After this the chamber is quickly cooled back to 15
325 °C. Figure 4b shows a time series of the Org/sulfate and ON^{aer} /sulfate ratios measured by the ACSM.
326 Sulfate has a low vapor pressure and does not evaporate significantly at the temperatures investigated;
327 therefore changes in the ON^{aer} /sulfate and Org/sulfate ratios with chamber temperature can be
328 attributed to partitioning of organic nitrates and other organic species between the gas and particle
329 phases or wall losses of gas-phase species. As Fig. 4b shows, Org/sulfate and ON^{aer} /sulfate decreased
330 with increasing temperature and increased with decreasing temperature, suggesting evaporation of
331 species at higher temperatures and their re-partitioning to the particle phase at lower temperatures.

332 Figure 4c shows the effects of temperature on various compounds measured in the gas phase. Several
333 organic compounds – with and without ON functional groups - increase with increasing temperature.
334 This suggests that these compounds are present in both the gas and particle phases and evaporate at
335 higher temperature resulting in increased gas phase concentrations. As temperature is increased the
336 percent change in the concentration of gas-phase $\text{C}_{10}\text{H}_{16}\text{O}_2$ is less than the change in $\text{C}_{10}\text{H}_{16}\text{O}_4$ and the
337 percent change in the concentration of gas-phase $\text{C}_{10}\text{H}_{15}\text{NO}_4$ is less than the change in $\text{C}_{10}\text{H}_{15}\text{NO}_6$. This is
338 consistent with the more highly oxidized compounds having a lower vapor pressure and evaporating
339 less. As the temperature is decreased back to 15 °C the concentrations return to the pre-heating trends,
340 suggesting that re-condensation to the particle-phase has occurred. These observations, as well as the
341 trends seen in particle-phase measurements, are consistent with equilibrium partitioning and
342 inconsistent with the irreversible partitioning of ON recently suggested by Perraud et al. (2012).

343 Other processes may influence particle and gas concentrations of organic compounds. Continuing
344 reactions with O₃ and nitrate radicals (since O₃ and NO₂ are both present) limit the ability to stop all
345 chemical activity. This is seen in the gas phase compounds, some of which appear to be changing in
346 concentration after the UV lights are off. Despite this a clear change is seen in all compounds with a
347 temperature increase. During the cooling phase (beginning at t = 320 minutes) the particle phase
348 organic and nitrate concentrations do not return to the original levels. It is likely that some organic
349 compounds are lost to the walls of the Teflon chamber, especially since they reach the coldest
350 temperatures during active cooling, and thus Org/sulfate does not return to the values seen before
351 temperature changes began. Despite these limitations it is clear that both the Org/sulfate and
352 ON^{aer}/sulfate ratios decrease with heating, consistent with semi-volatile organics and organic nitrates.

353 Table 1 summarizes the ON partitioning coefficient averaged over approximately 20 minutes from when
354 PM organics and nitrates peak in concentration. PM concentration and partitioning data are not
355 calculated for experiments above 60% RH. As discussed, these experiments had higher and less
356 consistent nitrate decay rates which may affect partitioning. There may also be issues in applying the
357 wall-loss and CE corrections used here and in previous work (Hildebrandt et al., 2009), which assume
358 that the particles measured by the SEMS before lights are turned on consist only of ammonium sulfate.
359 In these high RH experiments the particles may contain a significant fraction of water. The wall loss
360 correction also assumes that particles lost to the walls participate in partitioning as though they were
361 still in suspension. This assumption may be poor if small amounts of water condense onto the walls of
362 the chamber in these high RH experiments.

363 Data taken throughout the lower-concentration experiments (Expts 1, 2, and 3) with UV lights on were
364 fit to a volatility basis set as these experiments were conducted under conditions which are more
365 atmospherically relevant. Volatility basis set (VBS) parameters are static but are often used to
366 approximate dynamic systems such as the one observed in these experiments. Experimental data were
367 used after total PM organics (corrected for wall losses) had reached 2 μg m⁻³ to avoid effects of noise
368 and model uncertainty at the beginning of the experiments when concentrations of both gas- and
369 particle-phase organic nitrates were low. Outlying points (for example, when PM organics temporarily
370 rose above 2 μg m⁻³ but subsequent data suggested that condensation had not begun) were removed as
371 well. Figure 5 shows the data used to find the volatility basis set along with the fit. The C* values used for
372 this were 1, 10, 100, and 1000 μg m⁻³; the corresponding mass fractions (F_i) calculated to give the best
373 fit for Eq. (2) (Sect. 2.2) are F_i = 0, 0.11, 0.03, and 0.86.

374 As seen in Fig. 5 these results indicate that under typical ambient conditions (< 40 μg/m³ of OA) 5-10%
375 of organic nitrates formed from the photo-oxidation of α-pinene under high NO_x conditions are
376 expected to partition to the particle phase. This is significantly lower than the organic nitrate
377 partitioning calculated by Rollins et al. (2013) for organic nitrates measured in Bakersfield, CA during the
378 CalNex campaign in 2010. In those measurements >30% partitioning of ON was observed at organic
379 aerosol concentrations of 10 μg/m³. The difference could be attributed to differences in precursor
380 molecules and levels of oxidation. Studies have shown that high NO_x conditions can shift photochemical
381 oxidation products of terpenes towards higher volatility compounds (Wildt et al. 2014). Rollins et al.
382 determined using the SPARC model (Hilal et al., 2003) that precursor molecules (a mix of C5-C15 VOCs)

383 would need two stages of oxidative chemistry beyond the initial oxidation of the VOC to reach the point
384 when 19-28% would partition to the particle phase for a C_{OA} of $3 \mu\text{g m}^{-3}$. This may suggest that the ON
385 formed in our experiments have undergone fewer than three generations of oxidation as they are more
386 volatile than the ON measured in Bakersfield during CalNex 2010. It should also be noted that the
387 thermal dissociation-laser induced fluorescence (TD-LIF) instrument used by Rollins et al. (2013) has
388 been shown in a recent study to measure PM ON a factor of two higher than the ON measured by
389 aerosol mass spectrometers (Ayres et al., 2015) which utilize similar measurement and detection
390 techniques as the ACSM used in this work. While the reasons for this difference are unknown it would
391 result in a higher partitioning coefficient compared to the one calculated from the AMS (or ACSM) and
392 explain part of the observed difference.

393 **4 Conclusions**

394 Organic nitrates formed during the oxidation of α -pinene decay in the particle phase at a rate of 2 day^{-1}
395 when RH is between 20 and 60%; no significant decay was observed below 20% RH. During experiments
396 when the highest observed RH exceeded the deliquescence RH of the ammonium sulfate seed aerosol,
397 the particle-phase ON decay was as high as 7 day^{-1} and more variable. The dependence of observed
398 decay rate on relative humidity suggests organic nitrate hydrolysis as the most plausible explanation.
399 The gas-particle partitioning of ON determines their potential to hydrolyze. Partitioning of the ON is
400 reversible and can be described by a volatility basis set.

401 The conversion of NO_x to organic nitrates affects local ozone production. Partitioning and hydrolysis of
402 organic nitrates affect regional concentrations of organic particulate matter and ozone. The organic
403 nitrate partitioning coefficient and hydrolysis rates from this work can be used to include these
404 processes in chemical transport models and more accurately represent the effect of organic nitrates on
405 concentrations of ozone and particulate matter.

406 **5 Acknowledgements**

407 This work was funded in part through a grant from the Texas Commission on Environmental Quality
408 (TCEQ), administered by The University of Texas through the Air Quality Research Program (Project 12-
409 012). The contents, findings opinions and conclusions are the work of the authors and do not
410 necessarily represent findings, opinions or conclusions of the TCEQ. The work was also funded in part
411 with funds from the State of Texas as part of the program of the Texas Air Research Center. The
412 contents do not necessarily reflect the views and policies of the sponsor nor does the mention of trade
413 names or commercial products constitute endorsement or recommendation for use.

414 **6 References**

415
416 Allan, J. D., Delia, A. E., Coe, H., Bower, K. N., Alfarra, M. R., Jimenez, J. L., Middlebrook, A. M., Drewnick,
417 F., Onasch, T. B., Canagaratna, M. R., Jayne, J. T. and Worsnop, D. R.: A generalised method for the

418 extraction of chemically resolved mass spectra from Aerodyne aerosol mass spectrometer data, *J.*
419 *Aerosol Sci.*, 35(7), 909–922, doi:10.1016/j.jaerosci.2004.02.007, 2004.

420 Ayres, B. R., Allen, H. M., Draper, D. C., Brown, S. S., Wild, R. J., Jimenez, J. L., Day, D. A., Campuzano-
421 Jost, P., Hu, W., de Gouw, J., Koss, A., Cohen, R. C., Duffey, K. C., Romer, P., Baumann, K., Edgerton,
422 E., Takahama, S., Thornton, J. A., Lee, B. H., Lopez-Hilfiker, F. D., Mohr, C., Goldstein, A. H., Olson, K.
423 and Fry, J. L.: Organic nitrate aerosol formation via NO_x + BVOC in the Southeastern US, *Atmos.*
424 *Chem. Phys. Discuss.*, 15(12), 16235–16272, doi:10.5194/acpd-15-16235-2015, 2015.

425 Baker, J. and Easty, D.: Hydrolysis of Organic Nitrates, *Nature*, 166(4212), 156–156,
426 doi:10.1038/166156a0, 1950.

427 Baker, J. and Easty, D.: Hydrolytic Decomposition of Esters of Nitric Acid .1. General Experimental
428 Techniques - Alkaline Hydrolysis and Neutral Solvolysis of Methyl, Ethyl, Isopropyl, and Tert-Butyl
429 Nitrates in Aqueous Alcohol, *J. Chem. Soc.*, (APR), 1193–1207, doi:10.1039/jr9520001193, 1952.

430 Boschan, R., Mellow, R. T. and Van Dolah, R. W.: The Chemistry of Nitrate Esters, *Chem. Rev.*, 55(3),
431 485–510, doi:10.1021/cr50003a001, 1955.

432 Boyd, C. M., Sanchez, J., Xu, L., Eugene, A. J., Nah, T., Tuet, W. Y., Guzman, M. I. and Ng, N. L.: Secondary
433 organic aerosol formation from the β-pinene+NO₃ system: effect of humidity and peroxy radical fate,
434 *Atmos. Chem. Phys.*, 15(13), 7497–7522, doi:10.5194/acp-15-7497-2015, 2015.

435 Browne, E. C., Min, K.-E., Wooldridge, P. J., Apel, E., Blake, D. R., Brune, W. H., Cantrell, C. A., Cubison, M.
436 J., Diskin, G. S., Jimenez, J. L., Weinheimer, A. J., Wennberg, P. O., Wisthaler, A. and Cohen, R. C.:
437 Observations of total RONO₂ over the boreal forest: NO_x sinks and HNO₃ sources, *Atmos. Chem.*
438 *Phys.*, 13(9), 4543–4562, doi:10.5194/acp-13-4543-2013, 2013.

439 Carter, W., Cockeriii, D., Fitz, D., Malkina, I., Bumiller, K., Sauer, C., Pisano, J., Bufalino, C. and Song, C.: A
440 new environmental chamber for evaluation of gas-phase chemical mechanisms and secondary
441 aerosol formation, *Atmos. Environ.*, 39(40), 7768–7788, doi:10.1016/j.atmosenv.2005.08.040, 2005.

442 Chuang, W. K. and Donahue, N. M.: A two-dimensional volatility basis set – Part 3: Prognostic modeling
443 and NO_x dependence, *Atmos. Chem. Phys. Discuss.*, 15(12), 17283–17316, doi:10.5194/acpd-15-
444 17283-2015, 2015.

445 Darer, A. I., Cole-Filipiak, N. C., O’Connor, A. E. and Elrod, M. J.: Formation and stability of
446 atmospherically relevant isoprene-derived organosulfates and organonitrates., *Environ. Sci. Technol.*,
447 45(5), 1895–902, doi:10.1021/es103797z, 2011.

448 Day, D. A., Liu, S., Russell, L. M. and Ziemann, P. J.: Organonitrate group concentrations in submicron
449 particles with high nitrate and organic fractions in coastal southern California, *Atmos. Environ.*,
450 44(16), 1970–1979, doi:10.1016/j.atmosenv.2010.02.045, 2010.

451 Donahue, N. M., Robinson, A. L., Stanier, C. O. and Pandis, S. N.: Coupled partitioning, dilution, and
452 chemical aging of semivolatile organics., *Environ. Sci. Technol.*, 40(8), 2635–43,
453 doi:10.1021/es052297c, 2006.

454 Fry, J. L., Rollins, A. W., Wooldridge, P. J., Brown, S. S., Fuchs, H. and Dub, W.: Organic nitrate and
455 secondary organic aerosol yield from NO₃ oxidation of β -pinene evaluated using a gas-phase kinetics
456 / aerosol partitioning model, *Atmos. Chem. Phys.*, 9(3), 1431–1449, 2009.

457 Hilal, S., Karickhoff, S. and Carreira, L.: Prediction of the vapor pressure boiling point, heat of
458 vaporization and diffusion coefficient of organic compounds, *QSAR Comb. Sci.*, 22(6), 565–574,
459 doi:10.1002/qsar.200330812, 2003.

460 Hildebrandt, L., Donahue, N. M. and Pandis, S. N.: High formation of secondary organic aerosol from the
461 photo-oxidation of toluene, *Atmos. Chem. Phys.*, 9(9), 2973–2986, 2009.

462 Hildebrandt Ruiz, L. and Yarwood, G.: Interactions between Organic Aerosol and NO_y, Austin, TX.
463 Prepared for the Texas AQRP (Project 12-012), by the University of Texas at Austin, and ENVIRON
464 International Corporation, Novato, CA, available at: [http://aqrp.ceer.utexas.edu/
465 projectinfoFY12_13/12-012/12-012FinalReport.pdf](http://aqrp.ceer.utexas.edu/projectinfoFY12_13/12-012/12-012FinalReport.pdf), 2013.

466 Hildebrandt Ruiz, L., Paciga, A., Cerully, K., Nenes, A., Donahue, N. M. and Pandis, S. N.: Aging of
467 Secondary Organic Aerosol from Small Aromatic VOCs: Changes in Chemical Composition, Mass Yield,
468 Volatility and Hygroscopicity, *Atmos. Chem. Phys. Discuss.*, 14, 31441–31481, 2014.

469 Hu, K. S., Darer, A. I. and Elrod, M. J.: Thermodynamics and kinetics of the hydrolysis of atmospherically
470 relevant organonitrates and organosulfates, *Atmos. Chem. Phys.*, 11(16), 8307–8320,
471 doi:10.5194/acp-11-8307-2011, 2011.

472 Jacobs, M. I., Burke, W. J. and Elrod, M. J.: Kinetics of the reactions of isoprene-derived hydroxynitrates:
473 gas phase epoxide formation and solution phase hydrolysis, *Atmos. Chem. Phys.*, 14(17), 8933–8946,
474 doi:10.5194/acp-14-8933-2014, 2014.

475 Kebabian, P. L., Wood, E. C., Herndon, S. C. and Freedman, A.: A practical alternative to
476 chemiluminescence-based detection of nitrogen dioxide: Cavity attenuated phase shift spectroscopy,
477 *Environ. Sci. Technol.*, 42(16), 6040–6045, doi:10.1021/es703204j, 2008.

478 Lindinger, W., Hansel, A., Jordan, A. and Hansel, A.: Proton-transfer-reaction mass spectrometry (PTR –
479 MS): on-line monitoring of volatile organic compounds at pptv levels, *Chem. Soc. Rev.*, 27, 347–354,
480 1998.

481 Liu, S., Shilling, J. E., Song, C., Hiranuma, N., Zaveri, R. A. and Russell, L. M.: Hydrolysis of Organonitrate
482 Functional Groups in Aerosol Particles, *Aerosol Sci. Technol.*, 46(12), 1359–1369,
483 doi:10.1080/02786826.2012.716175, 2012.

484 Matsunaga, A. and Ziemann, P. J.: Gas-Wall Partitioning of Organic Compounds in a Teflon Film Chamber
485 and Potential Effects on Reaction Product and Aerosol Yield Measurements, *Aerosol Sci. Technol.*,
486 44(10), 881–892, doi:10.1080/02786826.2010.501044, 2010.

487 Ng, N. L., Chhabra, P. S., Chan, A. W. H., Surratt, J. D., Kroll, J. H., Kwan, A. J., McCabe, D. C., Wennberg,
488 P. O., Sorooshian, A., Murphy, S. M., Dalleska, N. F., Flagan, R. C. and Seinfeld, J. H.: Effect of NO_x

489 level on secondary organic aerosol (SOA) formation from the photooxidation of terpenes, *Atmos.*
490 *Chem. Phys. Discuss.*, 7(4), 10131–10177, doi:10.5194/acpd-7-10131-2007, 2007.

491 Ng, N. L., Herndon, S. C., Trimborn, A., Canagaratna, M. R., Croteau, P. L., Onasch, T. B., Sueper, D.,
492 Worsnop, D. R., Zhang, Q., Sun, Y. L. and Jayne, J. T.: An Aerosol Chemical Speciation Monitor (ACSM)
493 for Routine Monitoring of the Composition and Mass Concentrations of Ambient Aerosol, *Aerosol Sci.*
494 *Technol.*, 45(7), 780–794, doi:10.1080/02786826.2011.560211, 2011.

495 Pankow, J. F.: An absorption model of gas/particle partitioning of organic compounds in the
496 atmosphere, *Atmos. Environ.*, 28(2), 185–188, doi:10.1016/1352-2310(94)90093-0, 1994.

497 Perraud, V., Bruns, E. a, Ezell, M. J., Johnson, S. N., Yu, Y., Alexander, M. L., Zelenyuk, A., Imre, D., Chang,
498 W. L., Dabdub, D., Pankow, J. F. and Finlayson-Pitts, B. J.: Nonequilibrium atmospheric secondary
499 organic aerosol formation and growth., *Proc. Natl. Acad. Sci. U. S. A.*, 109(8), 2836–41,
500 doi:10.1073/pnas.1119909109, 2012.

501 Perring, A. E., Bertram, T. H., Wooldridge, P. J., Fried, A., Heikes, B. G., Dibb, J., Crouse, J. D., Wennberg,
502 P. O., Blake, N. J., Blake, D. R., Brune, W. H., Singh, H. B. and Cohen, R. C.: Airborne observations of
503 total RONO₂: new constraints on the yield and lifetime of isoprene nitrates, *Atmos. Chem. Phys.*, 9(4),
504 1451–1463, doi:10.5194/acp-9-1451-2009, 2009.

505 Rindelaub, J. D., McAvey, K. M. and Shepson, P. B.: The photochemical production of organic nitrates
506 from α -pinene and loss via acid-dependent particle phase hydrolysis, *Atmos. Environ.*, 100, 193–201,
507 doi:10.1016/j.atmosenv.2014.11.010, 2015.

508 Rollins, A. W., Pusede, S., Wooldridge, P., Min, K.-E., Gentner, D. R., Goldstein, A. H., Liu, S., Day, D. A.,
509 Russell, L. M., Rubitschun, C. L., Surratt, J. D. and Cohen, R. C.: Gas/particle partitioning of total alkyl
510 nitrates observed with TD-LIF in Bakersfield, *J. Geophys. Res. Atmos.*, 118(12), 6651–6662,
511 doi:10.1002/jgrd.50522, 2013.

512 Seinfeld, J. H. and Pandis, S. N.: *Atmospheric Chemistry and Physics*, 2nd ed., Wiley-Interscience,
513 Hoboken, 2006.

514 Wildt, J., Mentel, T. F., Kiendler-Scharr, A., Hoffmann, T., Andres, S., Ehn, M., Kleist, E., M \ddot{u} sgen, P.,
515 Rohrer, F., Rudich, Y., Springer, M., Tillmann, R. and Wahner, A.: Suppression of new particle
516 formation from monoterpene oxidation by NO_x, *Atmos. Chem. Phys.*, 14(6), 2789–2804,
517 doi:10.5194/acp-14-2789-2014, 2014.

518 Winer, A. M., Peters, J. W., Smith, J. P. and Pitts, J. N.: Response of Commercial Chemiluminescent NO-
519 NO Analyzers to Other Nitrogen-Containing Compounds, *Environ. Sci. Technol.*, 8(13), 1118–1121,
520 doi:10.1021/es60098a004, 1973.

521

522

523

524 Table 1. Experimental conditions and summary of results.

Exp	initial α - pinene (ppb)	initial NO (ppb)	RH (%)	H ₂ O ₂ conc in model (ppb) ^a	O ₃ (ppb) ^b	ON ^{aer} ($\mu\text{g}/\text{m}^3$) ^{b,c}	PM Org ($\mu\text{g}/\text{m}^3$) ^{b,c}	ON ^{gas} (ppb) ^b	Part coeff ^d	Hyd. (day ⁻¹)
1	40	30	22	100	90	7	90	13	0.19	NA ^e
2	40	40	39	60	50	6	60	11	0.18	2.2
3	40	40	0	40	50	4	30	13	0.10	NA ^e
4	130	110	68	600	210					2.4
5	130	130	22	900	330	70	780	57	0.33	1.8
6	130	120	50	500	240	40	460	47	0.26	1.9
7	130	120	15	200	210	50	510	34	0.38	0.2
8	80	80	0	1000	300	30	310	32	0.26	0.6
9	80	80	0	1500	330	20	270	28	0.25	0.2
10	50	50	70	600	180					6.9
11	40	40	70	200	70					2.5
12	50	50	67	500	170					5.2

525 ^a H₂O₂ concentration for which SAPRC model most closely matched measurements of NO_x and O₃

526 ^b Measured and averaged over a 20 minutes period when PM organics peaked

527 ^c Corrected for wall-losses as described in Sect. 2.1.2

528 ^d Molar basis

529 ^e Experimental conditions resulted in aerosol growth throughout the experiment

530

531

532

533

534

535

536

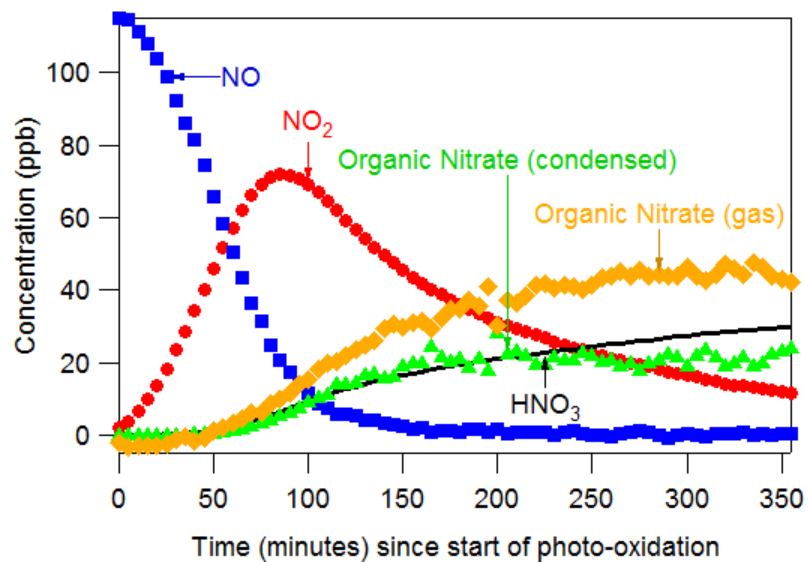
537

538

539

540

541



542

543 Figure 1 – Time series of oxidized-nitrogen species in Expt. 7. NO, NO₂, and ON^{aer} are measured directly.
 544 HNO₃ is modeled using SAPRC. ON^{gas} is calculated from a mass balance.

545

546

547

548

549

550

551

552

553

554

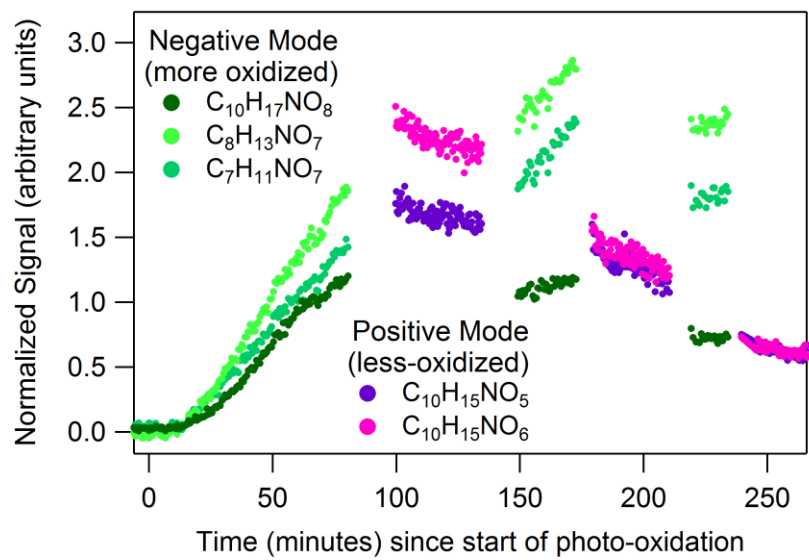
555

556

557

558

559



560

561

Figure 2 – Time series of selected organic nitrates identified by HR-ToF-CIMS (Expt. 10)

562

563

564

565

566

567

568

569

570

571

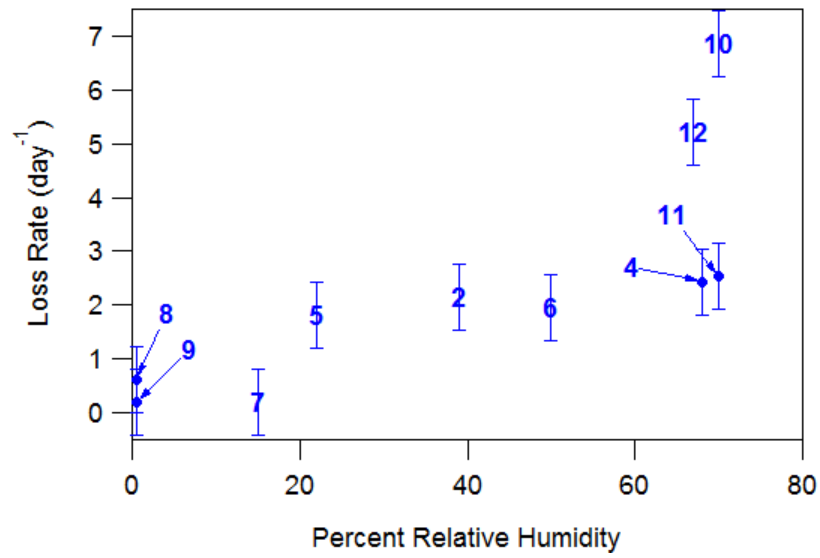
572

573

574

575

576



577

578 Figure 3. The organic nitrate loss rate as a function of relative humidity for Expts. 2, 4-12. Uncertainty
 579 (error bars) is estimated as 0.6 day⁻¹, the highest loss rate observed in experiments below 5% RH (Expt.
 580 8).

581

582

583

584

585

586

587

588

589

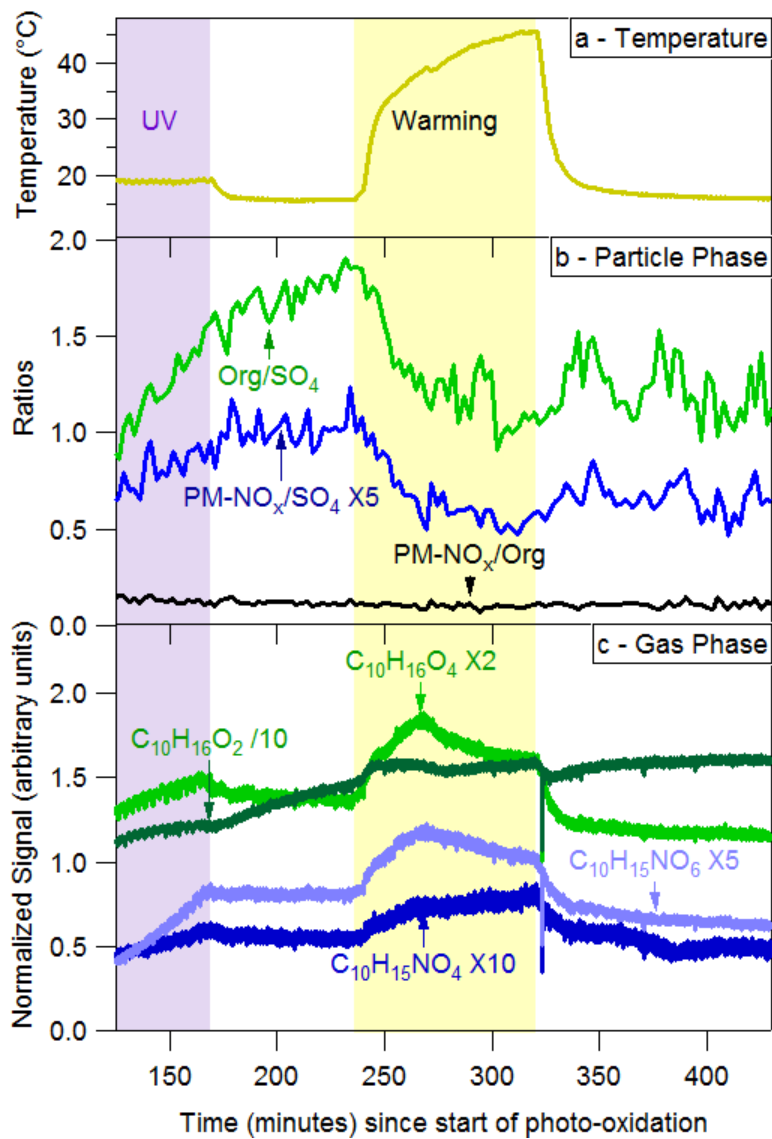
590

591

592

593

594



595

596

Figure 4 – Temperature effects on gas-particle partitioning of organic nitrates (Expt. 2).

597

598

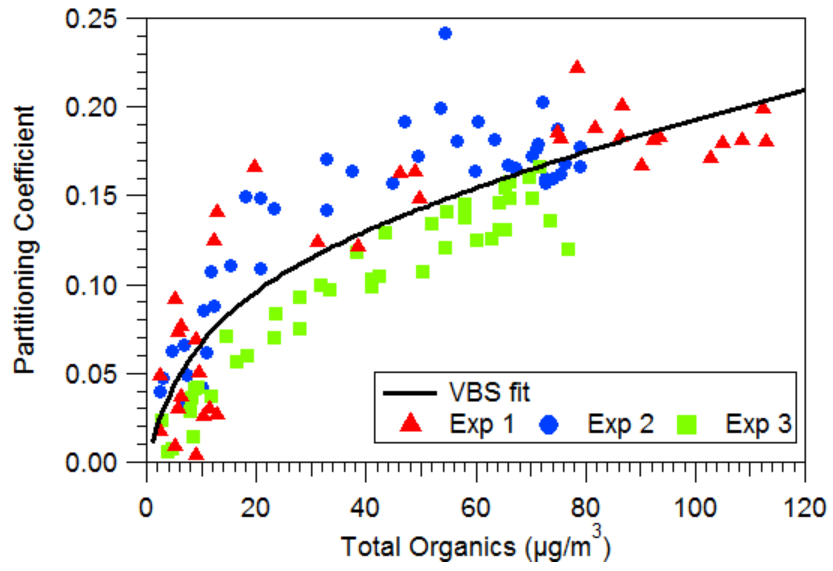
599

600

601

602

603



604

605

Figure 5 – Volatility basis set fit from this work shown with data from Expts. 1, 2, and 3.